

Dual-functional conjugated polymers based on trifluorene-2-yl-amine for RGB organic light-emitting diodes†

Hua Ye, Baofeng Zhao, Ming Liu, Xiao Zhou, Yanhu Li, Dongyun Li, Shi-Jian Su,* Wei Yang and Yong Cao

Received 25th July 2011, Accepted 30th August 2011

DOI: 10.1039/c1jm13533c

A series of blue-light-emitting conjugated polymers that possess high-lying HOMO energy levels were synthesized by introducing trifluorene-2-yl-amine (TFA) as a building block. The emission color could be effectively tuned in the region of deep-blue and light-blue by introducing various substituents onto the TFA as the pendants. Deep-blue light emission was achieved for the device based on P4FNCz as an emitting layer without using any hole-transport layer (HTL), giving a maximum current efficiency (CE) of 2.44 cd A⁻¹, corresponding to an external quantum efficiency of 3.00%, with Commission Internationale de L'Eclairage (CIE) coordinates of (0.16, 0.12). Thanks to the improved hole injection and transport ability, red- and green-light-emitting devices based on P4FNCz as an HTL were also successfully fabricated, giving a maximum CE of 7 and 25 cd A⁻¹ with CIE coordinates of (0.64, 0.34) and (0.29, 0.64), respectively, which are comparable to those of the devices based on a general HTL of 4,4'-bis(*N*-(1-naphthyl)-*N*-phenylamino)biphenyl (NPB). The CIE coordinates of the RGB devices are very close to those of the National Television System Committee (NTSC) and High Definition Television (HDTV) standard colors. The RGB devices achieved by tuning the carrier recombination zone with different electron-transport layers will facilitate the development of the polymer-based full-color flat-panel displays in an alternative process.

Introduction

Organic light-emitting diodes (OLEDs) have great potential applications in full-color flat-panel displays, back-lighting sources for liquid-crystal displays, and next-generation solid-state lighting sources.^{1–3} To realize commercialization of OLEDs in such applications, the development of high-efficiency and stable RGB emitters, especially for a blue one, remains a huge challenge.

Fluorene-based polymers and oligomers have been recognized as promising candidates for blue emitters due to their high photoluminescence (PL) efficiency, good chemical and thermal stability, film-forming ability, and high electroluminescence (EL) efficiency.⁴ However, the energy barrier for hole injection from the indium-tin oxide (ITO) anode to the fluorene-based polymers are quite high because of their low-lying highest occupied molecular orbital (HOMO) energy levels. In addition, because of

the large energy band-gaps of the fluorene-based blue-light emitters, it is also difficult to inject electrons from the cathode in blue OLEDs. To enhance the electron injection and transport, the introduction of electron-withdrawing components into the polymer has been proven to be effective.⁵ To achieve a reduced hole-injection barrier from the anode to the emitting layer (EML), poly(*N*-vinylcarbazole) (PVK) is generally utilized as a hole-transport layer (HTL) inserted between the anode and the EML.^{5–7} Liu *et al.* realized highly efficient blue OLEDs with Commission Internationale de L'Eclairage (CIE) coordinates of (0.16, 0.19) by using PVK as an HTL.⁵ With the same device configuration, Wang *et al.* reported deep-blue OLEDs based on a fluorescent π -conjugated dendrimer G0 with CIE coordinates of (0.155, 0.086).⁷ Although different solvents are utilized for spin-coating the HTL and EML, respectively, a mix of the two layers at the interface is unavoidable since PVK is soluble in the general organic solvents used for the EML. Moreover, the operating voltage of the devices with PVK as an HTL is higher than that of the devices without PVK, and this is a great disadvantage to achieving a high power conversion efficiency, a well-known factor that is crucially important to power consumption.

Another effective route is to modify their chemical structures in order to bring the HOMO energy levels closer to the work function of ITO,⁸ and thus to enhance the hole injection into the EML. Organic compounds containing triphenylamine (TPA) have been widely used as an HTL in organic electroluminescent

State Key Laboratory of Luminescent Materials and Devices (South China University of Technology) and Institute of Polymer Optoelectronic Materials and Devices, South China University of Technology, Guangzhou, 510640, China. E-mail: mssjsu@scut.edu.cn

† Electronic supplementary information (ESI) available: Detailed synthetic procedures, elemental analysis, and ¹H NMR spectroscopic characterizations of the polymers, UV-vis absorption and PL spectra of the polymers in dilute toluene solutions, cyclic voltammograms of the polymers, electroluminescent characteristics of the single-layer devices. See DOI: 10.1039/c1jm13533c

devices,⁹ and most organic compounds containing TPA units have high-lying HOMO energy levels (*ca.* -5.3 eV), which is very close to the work function of ITO and thus allows efficient hole injection.^{9c,10} To overcome the barrier for the hole injection of polyfluorenes (PFs), an effective approach is to modify their chemical structures through incorporating electron-donating moieties, such as TPA^{11a} and carbazole,^{11b} into the polymer main chain. Müllen *et al.* reported a PF derivative by introducing bulky TPA groups at the 9-position of fluorene as side chains.^{12a} End-capping the polymer chain with triaryl amines^{12b} or blocks bearing triarylamine pendants^{12c} is another alternative approach to introduce hole-transport units into the emitting polymers. The resultant polymers have the charge injection units distributed only at the ends of the chain,^{12b} where they are unable to affect the aggregation tendencies. Although a few electroluminescent TPA-based polymers have been developed, very strong and even only excimer emission was observed for the devices utilizing them as the emitters.^{12c,d} It is still a challenge to develop triarylamine-based polymers with improved hole injection and transport property and no aggregation/excimer emission.

Considering that the TPA derivatives usually exhibit morphological instabilities due to the non-rigid TPA molecular configuration,¹³ in this article, fluorene was chosen to replace benzene of TPA to give trifluorene-2-yl-amine (TFA) because of its ambipolar carrier transport property,¹⁴ high PL efficiency, and amorphous film-forming ability.⁴ A series of blue-light-emitting polymers based on a building block of TFA were developed and thoroughly characterized. To the best of our knowledge, this is the first report on conjugated polymers based on a building block of TFA. As expected, similar to the TPA-based polymers, HOMO energy levels of the TFA-based polymers are higher-lying than those of the PFs to give a reduced hole injection barrier. Due to the improved hole injection and transport ability, efficient blue-light-emitting devices were achieved by using the polymers as an EML without an HTL of PVK. In addition, their emission colors can be effectively tuned in the region of deep-blue and light-blue by introducing various substituents onto the TFA as the pendants. More importantly, red- and green-light-emitting devices were also successfully fabricated by using P4FNCz as an HTL, which are comparable to those based on a general HTL of 4,4'-bis(*N*-(1-naphthyl)-*N*-phenylamino)biphenyl (NPB). The RGB devices based on a single polymer achieved by the utilization of different electron-transport layers (ETL) for tuning the carrier recombination zone will facilitate the development of the polymer-based full-color flat-panel displays in an alternative process.

Results and discussion

Synthesis and chemical characterization

Take a consideration that the TFA unit is an electron donor. Various substituents, such as electron acceptors of cyano and oxadiazole groups and bipolar transporters of carbazole and *tert*-butyl substituted carbazole were introduced onto the TFA as the pendants to tune the HOMO and the lowest unoccupied molecular orbital (LUMO) energy levels of the polymers and thus to achieve a well-balanced carrier in the EML. The structures and synthetic routes of the TFA derivatives and the

corresponding polymers are outlined in Scheme 1 and Scheme 2, respectively. The four polymers of P4FN, P4FNcN, P4FNCz, P4FNtBuCz were synthesized by the palladium(0)-catalyzed Suzuki cross-coupling polycondensation of an equimolar mixture of two monomers of TFA derivatives (**11–14**) and **16**. In comparison, considering the relatively weak catalytic activity of Pd(PPh₃)₄, Pd(PPh₃)₄ was replaced by Pd(OAc)₂ and tricyclohexyl phosphine (PCy₃) for the preparation of P4FNOXDPh. The chemical structures of the polymers were verified by ¹H NMR and elemental analysis.

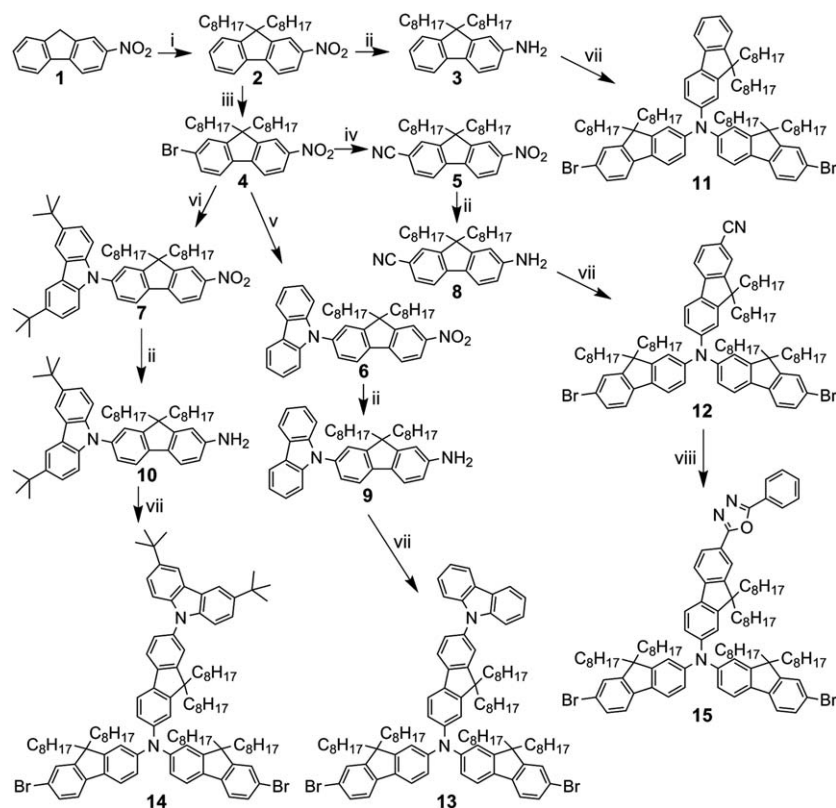
The developed TFA-based polymers are soluble in conventional organic solvents, like toluene, chloroform, and tetrahydrofuran (THF). Molecular weights of the polymers were determined by gel permeation chromatography (GPC) utilizing THF as a solvent and polystyrene as a standard. As shown in Table 1, the number-average molecular weights (M_n) of the polymers are from 17.5 to 27.8 kDa with a polydispersity index (PDI, weight-average molecular weight (M_w)/ M_n) between 1.67 and 3.86. The C, H and N contents for the five polymers are close to those calculated from the feed compositions.

Thermal properties

The thermal properties of the five polymers were determined by differential scan calorimetry (DSC) and thermogravimetric analysis (TGA) under a nitrogen atmosphere. As shown in Table 1, all the polymers exhibit good thermal stability with 5% weight-loss temperatures (T_d) around 420 °C due to the introduction of the bulky TFA building blocks into the main chain, which impart the chains with rigidity and non-coplanarity. With the change of the substituents at the C-7 position of the pendant fluorene of TFA, relatively high glass transition temperatures (T_g) ranging from 60 to 90 °C were achieved. For P4FNCz and P4FNtBuCz, which possess the bulky pendant of carbazole, a T_g up to 90 °C was achieved, which is 30 °C higher than that of P4FN without such a bulky pendant. Owing to the longer pendant of phenyl oxadiazole, the T_g of P4FNOXDPh increases to 78 °C compared with P4FN. Even for P4FNcN with the smallest substituent group of cyano, its T_g is 12 °C higher than that of P4FN. The increment of T_g in comparison with P4FN can be attributed to the different substituents at the pendant fluorene of TFA that induce the change in rigidity of polymer chain, polarity of the side chain, and thus the stronger molecular interaction.^{15a}

Optical properties

In toluene solution, the polymers exhibit one distinct absorption band at about 400 nm, which corresponds to the π - π^* transition of the conjugated polymer backbone (Fig. S1, see Supporting Information†).¹⁶ As a reference of P4FN, its absorption band peaks are at 404 nm. In comparison, the absorption bands for P4FNCz and P4FNtBuCz are slightly narrower than that of P4FN combined with a broad absorption band in the range of 300~350 nm, which can be attributed to the pendant carbazole. By introducing electron-withdrawing cyano and phenyl oxadiazole as the pendants, bathochromic shifts of 4 and 10 nm were observed for P4FNcN and P4FNOXDPh, respectively, due to the intramolecular charge-transfer (ICT) interaction between the electron-withdrawing cyano and oxadiazole and the

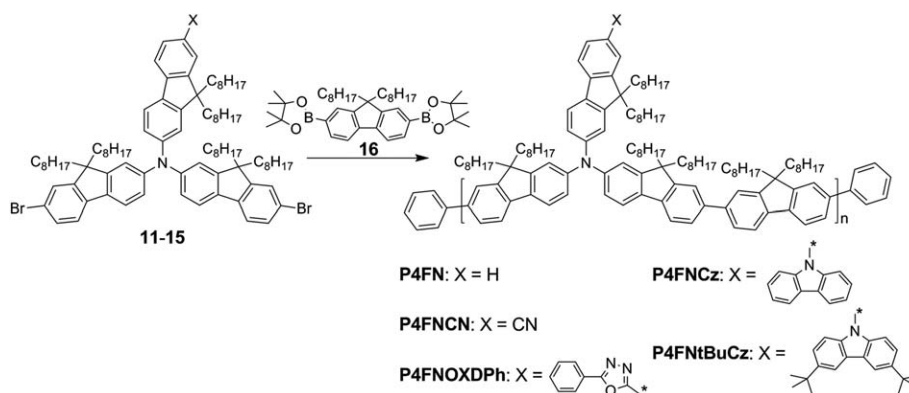


Scheme 1 Synthetic routes of the trifluorene-2-yl amine (TFA) derivatives. *Reagents and conditions:* i: $n\text{-C}_8\text{H}_{17}\text{Br}$, toluene, 50% NaOH, Bu_4NBr , 60°C ; ii: hydrazine monohydrate, 5% Pd/C, EtOH, reflux; iii: iron, CHCl_3 , Br_2 , 0°C ; iv: CuCN , DMF, reflux; v: carbazole, Cu, K_2CO_3 , DMSO, 150°C ; vi: 3,6-di-*tert*-butyl-9*H*-carbazole, CuI, K_2CO_3 , 18-crown-6, DMPU, 180°C ; vii: 2,7-dibromo-9,9-dioctylfluorene, $\text{Pd}_2(\text{dba})_3$, DPPF, *t*-BuONa, toluene, 110°C ; viii: 1) NaN_3 , NH_4Cl , anhydrous DMF, 100°C ; 2) benzencarbonyl chloride, anhydrous pyridine, reflux.

electron-donating TFA, giving reduced energy band-gaps. For the films, besides the absorption bands at ~ 400 nm, another intense band is observed at ~ 220 nm (Fig. 1(a)), which can be attributed to the $n\text{-}\pi^*$ transitions of fluorene. These absorption bands are absent for the solutions since they are overlapped by the absorption of toluene. Two specific bands of 313 and 332 nm were observed for P4FNOXDPh, and they can be attributed to the $\pi\text{-}\pi^*$ transitions of the phenyl oxadiazole pendant. For P4FNCz and P4FNTtBuCz, two absorption bands were observed

Table 1 Molecular weights and thermal properties of the polymers

Polymer	M_n/kDa	M_w/kDa	PDI	$T_d/^\circ\text{C}$	$T_g/^\circ\text{C}$
P4FN	23.2	59.0	2.55	415	60
P4FNCN	17.5	32.2	1.84	421	72
P4FNCz	26.3	43.8	1.67	416	89
P4FNTtBuCz	20.9	37.5	1.80	423	90
P4FNOXDPh	27.8	107	3.86	422	78



Scheme 2 Synthetic route of the polymers based on trifluorene-2-yl amine (TFA). *Reagents and conditions:* $\text{Pd}(\text{PPh}_3)_4$ or $\text{Pd}(\text{OAc})_2/\text{PCy}_3$, toluene, Et_4NOH , deionized water, $90\text{--}100^\circ\text{C}$.

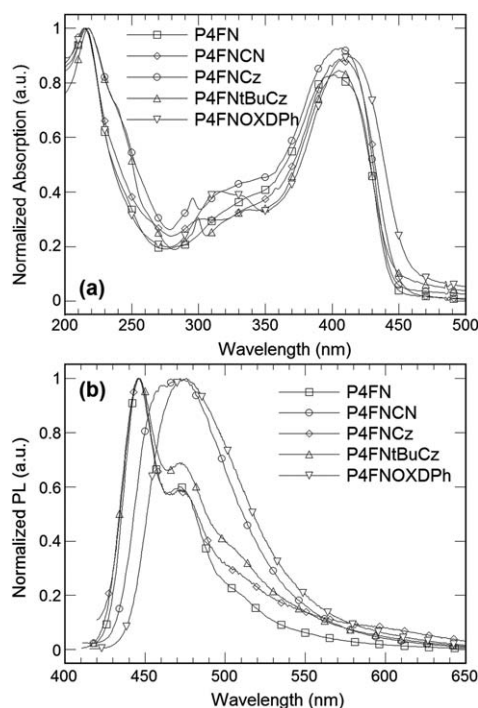


Fig. 1 Normalized UV-vis absorption (a) and PL (b) spectra of the polymers in thin films.

at 295 and 300 nm, respectively, which can be attributed to the π - π^* transitions of the pendant carbazole.

Similar bathochromic shifts were also observed for their PL spectra recorded in both toluene solution and thin film. For the toluene solutions of P4FN, P4FNCz, and P4FNtBuCz, their PL spectra peak at 442 nm with a shoulder at 470 nm (Fig. S2, see Supporting Information†). In comparison, PL spectrum of P4FNCN solution shifts to the longer wavelength and peaks at 446 nm, which can be attributed to the ICT interaction formed between the electron-donor of TFA and the electron-acceptor of cyano. The PL band of P4FNOXDPh solution shifts further to the longer wavelength, which can also be explained by the strong electron affinity of the oxadiazole component and the ICT interaction between the electron-donating segments of TFA and the electron-acceptor of the oxadiazole component. Moreover, the oxadiazole unit does not interrupt the π conjugation of TFA to the benzene unit,¹⁷ and P4FNOXDPh exhibits a red-shifted PL spectrum due to the elongated π conjugation in the side chain in comparison to the other polymers. As compared with the PL spectra of the polymers in toluene solution, the PL spectra of the polymers in thin films are slightly red-shifted (Fig. 1(b)), which can probably be ascribed to the aggregation and dielectric environment of the solid film.¹⁵

Electrochemical properties

The electrochemical properties of the polymers were investigated by cyclic voltammetry (CV) with a platinum working electrode and a platinum wire counter electrode at a scan rate of 50 mV s⁻¹ against a saturated calomel electrode (SCE) reference electrode with an argon saturated anhydrous solution of 0.1 mol L⁻¹ Bu₄NPF₆ in acetonitrile. The redox potential ($E_{1/2}$) of

ferrocene/ferrocenium (Fc/Fc⁺) measured to the SCE reference electrode under the same experimental conditions is -0.462 V. Note that the redox potential of Fc/Fc⁺ has an absolute energy level of -4.8 eV to vacuum,^{18b,c} and the redox potential of Fc/Fc⁺ should be 0.4 V vs. SCE. As thus, the potentials were calibrated to the Fc/Fc⁺ external standard by positively shifting in 0.862 V.¹⁹ The HOMO energy levels are calculated according to the following equations:^{18a} HOMO = -e (E_{ox} + 4.4) (eV), where E_{ox} is the onset oxidation potential. The LUMO energy levels of the polymers are estimated from the HOMO energy levels and the optical energy band-gaps. The energy band-gaps of the polymers are estimated from the absorption edges of the UV-vis spectra of the thin films (Table 2). As anticipated, the HOMO energy levels of all the TFA-based polymers are about -5.4 eV, which is nearly 0.5 eV higher-lying compared to the PFs (HOMO energy level is as low as -5.9 eV),²⁰ thus rendering efficient hole-injection from the anode. With introducing two *tert*-butyl groups at the 3-, and 6-positions of the carbazole component in P4FNCz, slightly reduced HOMO and LUMO energy levels were achieved for P4FNtBuCz. As is well-known, the *tert*-butyl group involves little electron affinity, and they do not participate in the π conjugation of the TFA main chain or the carbazole component. Additionally, according to the absorption edges of the solid films, the energy band-gap of P4FNCz is estimated to be 2.80 eV, which is equal to that of P4FNtBuCz. Although π - π stacking of the pendant carbazoles in P4FNtBuCz might be reduced due to the bulky *tert*-butyl group, the lowest energy absorption band according to the polymer backbone may be hardly influenced to give similar energy band-gaps. The decreased HOMO and LUMO energy levels of P4FNtBuCz can be attributed to the *tert*-butyl groups that might break the π - π stacking of carbazoles and fluorenes. Taking P4FN as a reference, slightly higher-lying HOMO and LUMO energy levels were achieved for P4FNCz. It can be attributed to the introduction of the electron-donor of carbazole at the pendant. In contrast, slightly reduced HOMO and LUMO energy levels were achieved for P4FNCN and P4FNOXDPh due to the introduction of the electron-acceptors of cyano and oxadiazole at the pendant.

Electroluminescence

To evaluate their electroluminescence properties, double-layer devices with a configuration of ITO/PEDOT:PSS (40 nm)/EML (70~80 nm)/TPBI (30 nm)/CsF (1.5 nm)/Al were fabricated,

Table 2 Energy band-gaps and electrochemical properties of the polymers

Polymer	Energy band-gap ^a /eV	E_{ox} ^b /V	HOMO ^c /eV	LUMO ^d /eV
P4FN	2.79	0.98	-5.38	-2.59
P4FNCN	2.77	1.04	-5.44	-2.67
P4FNCz	2.80	0.95	-5.35	-2.55
P4FNtBuCz	2.80	1.04	-5.44	-2.64
P4FNOXDPh	2.72	1.01	-5.41	-2.69

^a Estimated from the absorption edges of the polymer films. ^b E_{ox} is the onset oxidation potential that is calibrated to the Fc/Fc⁺ external standard. ^c Calculated according to HOMO = -e (E_{ox} + 4.4). ^d Calculated from the HOMO energy level and the energy band-gap.

where the polymers were used as an EML and TPBI (2,2',2''-(1,3,5-benzenetriyl)-tris-(1-phenyl-1*H*-benzimidazole)) is used as an electron-transport and hole-block layer to enhance the electron-injection/transport into the EML and to confine carrier recombination in the EML.

As shown in Fig. 2(a), the device based on P4FNCz exhibits the highest current density. It can be attributed to its relatively high-lying HOMO energy level that facilitates hole-injection from the anode. The current density of the device based on P4FNtBuCz is lower than that of the device based on P4FNCz. Taking into consideration that the only structural difference between these two polymers is that P4FNtBuCz possesses two *tert*-butyl groups at the 3- and 6-positions of the pendant carbazole component, the bulky *tert*-butyl groups may inhibit the π - π stacking of carbazoles and fluorenes and thus induce a reduced carrier transport property. A similar phenomenon was also found for the single-layer devices without using TPBI (Fig. S3, see Supporting Information†). As shown in Table 3, turn-on voltages (V_{on}) for electroluminescence (a luminance of 1 cd m^{-2} was detected) of the double-layer devices are between 2.9 and 3.5 V, and further lower V_{on} values of 2.8~3.3 V were achieved for the single-layer devices. In comparison, some of the previously reported blue OLEDs generally use PVK as an HTL

but show much higher V_{on} values of 4.8~5.8 V.⁵ Note that no such HTL is used for the current devices. The reduced driving voltage can be attributed to the introduction of TFA as a building block of the polymers that gives a higher-lying HOMO energy level and thus facilitates hole injection and transport from the anode.

The current efficiency (CE) *versus* current density characteristics of the double-layer devices are shown as Fig. 2(b). The device based on P4FN exhibits a maximum CE of 1.08 cd A^{-1} , which is the lowest one among all the double-layer devices. The relatively low efficiency can be attributed to the low carrier balance achieved in the device since P4FN is comprised of only the electron-donor of TFA. Due to this reason, the single-layer device based on P4FN exhibits a further lower maximum CE of 0.15 cd A^{-1} , since there is no TPBI that acts as a hole-block layer to give a further reduced carrier balance. Both the EL spectra of the single-layer device and the double-layer device show peaks at 445 nm with a subsidiary peak at 471 nm, which is consistent with its PL spectrum in film, indicating that both EL and PL emissions mostly arise from the same excited state or the same type of excitons.²¹ However, different from the double-layer device, a long tail was found in the EL spectrum at wavelengths longer than 500 nm for the single-layer device (Fig. S5, see Supporting Information†), which is absent in the PL spectrum. Note that the LUMO and HOMO energy levels of TPBI are -2.7 and -6.2 eV , respectively.²² For the double-layer devices, hole extraction from the EML to the cathode can be effectively impeded by such a deep HOMO energy level, thus enhancing the recombination probability of holes and electrons to form emissive excitons in the EML.²³ In contrast, it is anticipated that the carrier recombination zone in the single-layer device should be close to the cathode because of the relatively high-lying HOMO energy level and hole transport capacity of TFA. As thus, it is speculated that the long tail found for the P4FN-based single-layer device should be according to the excimer formed at the interface of P4FN and the cathode. But compared with the previously reported TPA-based polymer that shows only excimer emission,^{12d} the excimer emission is significantly suppressed by solely introducing fluorene instead of benzene as building blocks.

By introducing carbazole at the pendant fluorene of P4FN to give P4FNCz, significantly improved efficiency was achieved to give a maximum CE of 2.44 cd A^{-1} , corresponding to an external quantum efficiency (EQE) of 3.00% (Fig. 2(b)). Compared with the best value previously reported for the polymer-based pure blue OLEDs by using a single-layer device structure ($\text{CE}_{\text{max}} = 4.57 \text{ cd A}^{-1}$, $\text{EQE}_{\text{max}} = 4.54\%$),²⁴ the efficiency is slightly lower, but the current device exhibits a $\sim 1 \text{ V}$ lower turn-on voltage. Since carbazole is a well-known bipolar transporter, the introduction of carbazole as the pendant may facilitate both the hole and electron transport in the EML to give an improved current density and reduced driving voltage. In addition, the carrier balance was also improved to give an improved CE. A similar phenomenon was also found for the corresponding single-layer device. Aside from the improved efficiency, the improved electron transport also induces the carrier recombination zone apart from the interface of the EML and cathode for the single-layer device, restraining the formation of the excimer at the interface of the EML and cathode to give an improved color purity with CIE coordinates of (0.19, 0.20). A slightly lower CE was obtained for

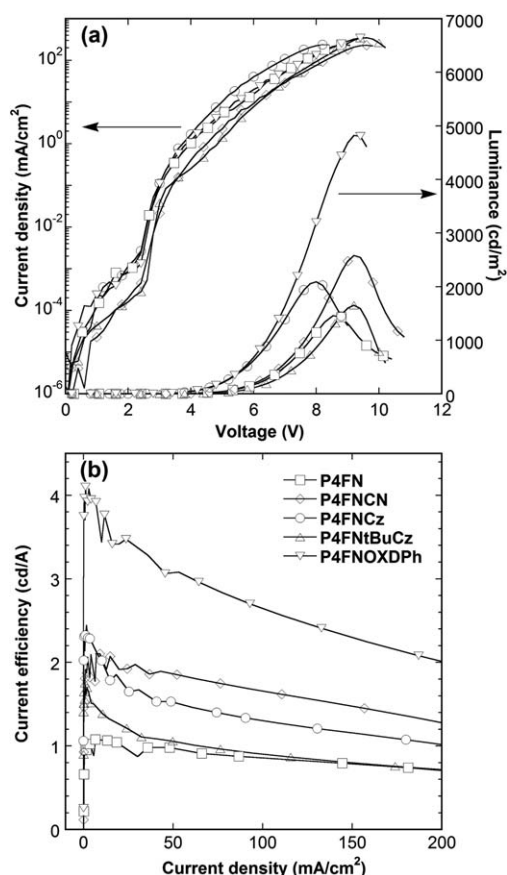


Fig. 2 (a) Current density and luminance *versus* voltage and (b) current efficiency *versus* current density characteristics of the double-layer devices with the configuration of ITO/PEDOT:PSS (40 nm)/EML (70~80 nm)/TPBI (30 nm)/CsF (1.5 nm)/Al. EML: P4FN (□), P4FNCN (◇), P4FNCz (○), P4FNtBuCz (△), and P4FNOXDPh (▽).

Table 3 Summary of the electroluminescent performance of the double-layer devices with the configuration of ITO/PEDOT:PSS (40 nm)/EML (70~80 nm)/TPBI (30 nm)/CsF (1.5 nm)/Al

EML	V_{on}^a/V	$L_{\text{max}}/\text{cd m}^{-2}$	$\text{CE}_{\text{max}}/\text{cd A}^{-1}$	$\text{EQE}_{\text{max}}(\%)$	CIE (x, y)
P4FN	3.3	1462	1.08	1.15	(0.16, 0.12)
P4FNCN	3.5	2583	2.10	1.76	(0.19, 0.27)
P4FNCz	2.9	2092	2.44	3.00	(0.16, 0.12)
P4FNtBuCz	3.2	1653	1.70	1.53	(0.18, 0.19)
P4FNOXDPH	2.9	4824	4.10	2.80	(0.18, 0.30)

^a Turn-on voltage for electroluminescence (a luminance of 1 cd m^{-2} was detected).

the double-layer device based on P4FNtBuCz in contrast to the device based on P4FNCz, and the decreased efficiency can be attributed to the reduced carrier transport property and thus the carrier balance.

Compared with the device based on P4FN, improved efficiency was also achieved for the device based on P4FNCN, giving a maximum CE of 2.10 cd A^{-1} , corresponding to an EQE of 1.76%. The improved efficiency can be attributed to the introduction of the electron-acceptor of cyano that gives the polymer a lower-lying LUMO energy level and thus a lower electron injection barrier. As thus, an improved carrier balance was achieved to give an improved efficiency. Further higher efficiency of 4.1 cd A^{-1} was achieved for the device based on P4FNOXDPH, and it can be attributed to its relatively lower-lying LUMO energy level (−2.69 eV) that is very close to that of TPBI (−2.70 eV) to give a reduced electron injection barrier from TPBI.²² The EL spectra of the double-layer devices based on the P4FNCN and P4FNOXDPH have peaks at 471 and 474 nm (Fig. 3), respectively, with smaller full-width at half-maximum (FWHM) values compared with the EL spectra of the corresponding single-layer devices. Similar to the PL spectra, bathochromic shifts were also observed in the EL spectra compared with the device based on P4FN, and it can be attributed to the strong electron affinity of the electron-acceptors of cyano and oxadiazole that induces an ICT interaction with the electron-donor of TFA. Owing to the ICT interaction, the emission colors could be effectively tuned in the region of deep-blue with CIE coordinates of (0.16, 0.12) and light-blue with CIE coordinates of (0.18, 0.30) by introducing various substituents onto the TFA as

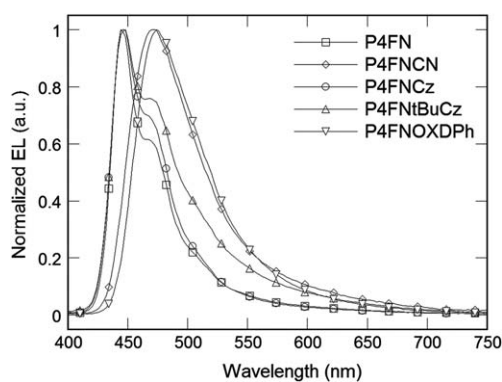


Fig. 3 EL spectra of the double-layer devices based on the polymers as an EML in the configuration of ITO/PEDOT:PSS (40 nm)/EML (70~80 nm)/TPBI (30 nm)/CsF (1.5 nm)/Al.

the pendants (Table 3). In addition, CIE coordinates of the deep-blue devices are close to the National Television System Committee (NTSC) and High Definition Television (HDTV) standard blue with CIE coordinates of (0.16, 0.07) and (0.15, 0.06), respectively.

Considering that the devices based on P4FNCz exhibit the lowest driving voltage and the highest EQE among these polymers in both single-layer and double-layer configurations, it is anticipated that P4FNCz should possess a good hole injection and transport ability to be used as an HTL for OLEDs, although few fluorene-based polymers have been reported as an emitting material as well as a hole-transport material to date. In addition, different from the previously mentioned color-tuning methodology of molecular design, it might also be possible to tune the emission color of the device by device engineering, the tuning of the carrier recombination zone with the polymers as an HTL. To validate this idea, the following two devices with configurations of ITO/PEDOT:PSS (40 nm)/P4FNCz (50 nm)/Alq3:DCJTB (3 wt%) (30 nm)/Alq3 (20 nm)/LiF (1 nm)/Al and ITO/PEDOT:PSS (40 nm)/P4FNCz (50 nm)/Alq3:C545T (1 wt%) (30 nm)/Alq3 (20 nm)/LiF (1 nm)/Al were fabricated, where P4FNCz is expected to be utilized as an HTL. DCJTB is 4-(dicyanomethylene)-2-*tert*-butyl-6-(1,1,7,7-tetramethyljulolidin-4-yl-vinyl)-4*H*-pyran, a well-known red-light-emitting dye, and C545T is 10-(2-benzothiazolyl)-2,3,6,7-tetrahydro-1,1,7,7-tetramethyl-1*H*,5*H*,11*H*-(1) benzopyrroprano(6,7-8-*I*_j) quinolizin-11-one, a well-known green-light-emitting dye. In these configurations, tris(8-hydroxyquinoline)aluminium (Alq3) is used as the host for the dyes as well as the ETL. Note that the HOMO energy level of Alq3 is −5.70 eV, which is only 0.35 eV lower-lying than that of P4FNCz. Different from the previously used TPBI, it is expected that holes can be easily injected into the co-deposited layer of Alq3 and dye from P4FNCz, and the carrier recombination in the co-deposited layer will excite the dye to give its emission. For comparison, a well-known hole-transport material of (4,4'-bis(*N*-(1-naphthyl)-*N*-phenylamino)-biphenyl) (NPB) was also used as an HTL instead of P4FNCz to give two devices as the references.

As shown in Fig. 4(a), for the devices based on DCJTB, the current density of the device based on P4FNCz is almost consistent with that of the device based on NPB. For the devices based on C545T, although the current density of the device based on P4FNCz is somewhat lower than that of the device based on NPB at voltages higher than 3 V, the same threshold voltage (V_{th}) of 2.2 V for current was achieved for both the devices. It indicates that holes can also be effectively injected from the anode when P4FNCz is used as an HTL instead of NPB. As shown in Fig. 4(b), for the devices based on C545T, a maximum

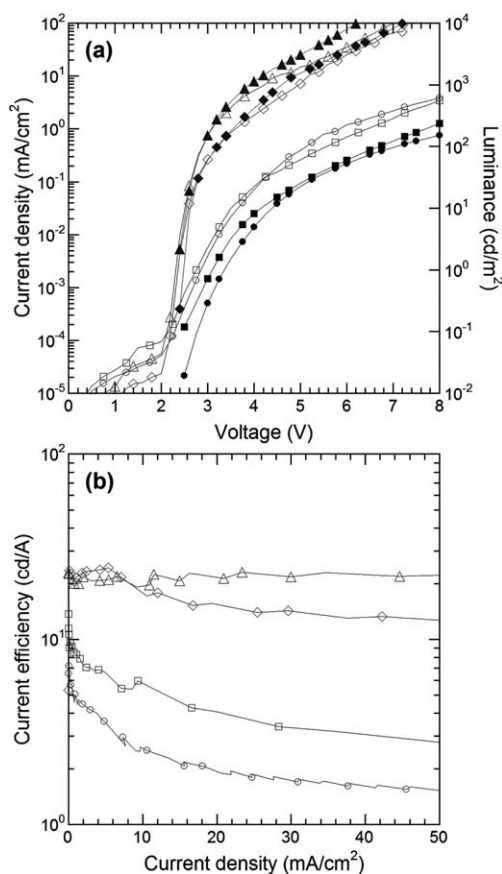


Fig. 4 Current density (closed symbols) and luminance (open symbols) versus voltage (a) and current efficiency (CE) versus current density (b) characteristics of devices with the configurations of ITO/PEDOT:PSS (40 nm)/P4FNCz (○) or NPB (□) (50 nm)/Alq3:DCJTBA (3 wt%) (30 nm)/Alq3 (20 nm)/LiF (1 nm)/Al and ITO/PEDOT:PSS (40 nm)/P4FNCz (◇) or NPB (△) (50 nm)/Alq3:C545T (1 wt%) (30 nm)/Alq3 (20 nm)/LiF (1 nm)/Al.

CE of 25 cd A⁻¹ was achieved for the device based on P4FNCz, which is comparable to that of the device based on NPB and is very close to the best value of the C545T-based devices previously reported (29.8 cd A⁻¹).²⁵ For the devices based on DCJTBA, a maximum CE of 7 cd A⁻¹ was achieved for the device based on P4FNCz, which is lower than that of the device based on NPB, and it can be attributed to the reduced carrier balance in the EML.

EL spectra of the devices based on P4FNCz are quite similar to those of the devices based on NPB, and no emission from P4FNCz or Alq3 was detected (Fig. 5). It further indicates efficient hole injection from P4FNCz to the EML for carrier recombination and effective energy transfer from Alq3 to the dyes. In addition, CIE coordinates of the devices based on C545T and DCJTBA are (0.29, 0.64) and (0.64, 0.34), respectively, which are very close to the NTSC standard green (0.31, 0.60) and red (0.63, 0.34) and HDTV standard green (0.30, 0.60) and red (0.64, 0.33). It proves that color-tuning can also be achieved by using P4FNCz as an HTL through the tuning of the carrier recombination zone by utilizing an appropriate ETL. The current findings will enable us to develop the polymer-based full-color flat-panel in an alternative process.

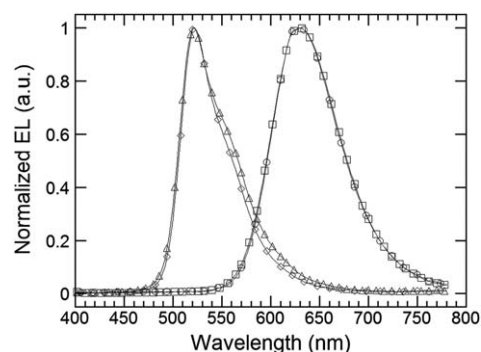


Fig. 5 EL spectra of the devices with the configurations of ITO/PEDOT:PSS (40 nm)/P4FNCz (○) or NPB (□) (50 nm)/Alq3:DCJTBA (3 wt%) (30 nm)/Alq3 (20 nm)/LiF (1 nm)/Al and ITO/PEDOT:PSS (40 nm)/P4FNCz (◇) or NPB (△) (50 nm)/Alq3:C545T (1 wt%) (30 nm)/Alq3 (20 nm)/LiF (1 nm)/Al.

Conclusions

In summary, a series of blue-light-emitting polymers based on a building block of TFA were synthesized *via* the palladium-catalyzed Suzuki coupling polycondensation. Their emission colors could be effectively regulated in the region of deep-blue and light-blue by solely changing the substituents at the pendant fluorene of TFA. Efficient hole injection from the anode to the polymers was achieved even without any HTL due to their high-lying HOMO energy level achieved by the introduction of the electron-donor of TFA. Efficient deep-blue light emission was observed for the device based on P4FNCz as an EML that shows a maximum CE of 2.44 cd A⁻¹, corresponding to an EQE of 3.00%, with CIE coordinates of (0.16, 0.12). Thanks to the improved hole injection and transport, red- and green-light-emitting devices were also successfully fabricated by using P4FNCz as an HTL, giving maximum CE values of 7 and 25 cd A⁻¹, respectively, which are comparable to the ones based on NPB as an HTL. Moreover, the CIE coordinates of the RGB devices are very close to those of the NTSC and HDTV standard colors, indicating that color-tuning achieved by the molecular design as well as the tuning of the carrier recombination zone will facilitate the development of the polymer-based full-color flat-panel in an alternative process.

Experimental

Measurement and characterization

¹H NMR and ¹³C NMR spectra were recorded on a Bruker AV-300 (300 MHz) in deuterated chloroform (CDCl₃) with tetramethylsilane as a reference. *M_n* and *M_w* were determined by a Waters GPC 2410 in THF using a calibration curve with standard polystyrene as a reference. Elemental analysis was performed on a Vario EL elemental analysis instrument (Elementar Co.). DSC measurements were performed on a Netzsch DSC 204 under N₂ flow at a heating rate of 10 °C min⁻¹ and a cooling rate of 20 °C min⁻¹. TGA measurements were performed on a Netzsch TG 209 under N₂ flow at a heating rate of 10 °C min⁻¹. UV-vis absorption spectra were recorded on a HP 8453 spectrophotometer. PL spectra were measured using

a Jobin-Yvon spectrofluorometer. CV was performed on a CHI600D electrochemical workstation with a platinum working electrode and a platinum wire counter electrode at a scan rate of 50 mV s^{-1} against an SCE reference electrode in an argon saturated anhydrous acetonitrile solution of 0.1 mol L^{-1} tetrabutylammonium hexafluorophosphate (Bu_4NPF_6). The polymer films for electrochemical measurements were coated from their toluene solutions.

Device fabrication and characterization

The fabrication process of the devices is as the following. ITO-coated glass substrates were cleaned by ultrasonic treatment in deionized water, acetone, detergent, and isopropyl alcohol sequentially. After treatment with oxygen plasma, a 40-nm-thin layer of poly-(3,4-ethylenedioxythiophene):poly(styrene sulfonate) (PEDOT:PSS) (Bayer Baytron P 4083) was spin-coated as a buffer layer. After being dried in a vacuum oven at $80 \text{ }^\circ\text{C}$ for 12 h, the xylene solutions of the polymers prepared in a nitrogen-filled drybox were spin-coated on the top of the PEDOT:PSS film. The thickness of the spin-coated film was controlled by regulating the spinning speed and the solution concentration, measured with an Alfa Step 500 surface profiler (Tencor). The low mass materials were vacuum deposited in a vacuum of $1 \times 10^{-4} \text{ Pa}$. A thin layer of CsF (1.5 nm) or LiF (1 nm) and subsequently 120-nm-thin layer of Al were vacuum deposited in a vacuum of $1 \times 10^{-4} \text{ Pa}$ as the cathode. Device performances were measured inside a drybox. Current density *versus* driving voltage characteristics were recorded with a Keithley 236 source meter. EL spectra were obtained by Oriel Instaspec IV CCD spectrograph. Luminance was measured by a PR 705 photometer (Photo Research). External quantum efficiencies were determined by a Si photodiode with calibration in an integrating sphere (IS080, Labsphere).

Acknowledgements

The authors greatly appreciate the financial support from the National Natural Science Foundation of China (Project No. 51073057), the Ministry of Science and Technology (Project No. 2009CB930604 and 2011AA03A110), and the Fundamental Research Funds for the Central Universities (2011ZZ0002).

References

- 1 J. H. Burroughes, D. D. C. Bradley, A. R. Brown, R. N. Marks, K. Mackay, R. H. Friend, P. L. Burns and A. B. Holmes, *Nature*, 1990, **347**, 539.
- 2 (a) B. W. D'Andrade and S. R. Forrest, *Adv. Mater.*, 2004, **16**, 1585; (b) A. C. Grimsdale, K. L. Chan, R. E. Martin, P. G. Jokisz and A. B. Holmes, *Chem. Rev.*, 2009, **109**, 897; (c) A. Misra, P. Kumar, M. N. Kamalasanan and S. Chandra, *Semicond. Sci. Technol.*, 2006, **21**, R35.
- 3 (a) R. H. Friend, R. W. Gymer, A. B. Holmes, J. H. Burroughes, R. N. Marks, C. Taliani, D. D. C. Bradley, D. A. Dos Santos, J. L. Bredas, M. Logdlund and W. R. Salaneck, *Nature*, 1999, **397**, 121; (b) M. A. Baldo, M. E. Thompson and S. R. Forrest, *Nature*, 2000, **403**, 750.
- 4 (a) Q. Pei and Y. Yang, *J. Am. Chem. Soc.*, 1996, **118**, 7416; (b) U. Scherf and E. J. W. List, *Adv. Mater.*, 2002, **14**, 477; (c) M.-C. Hung, J.-L. Liao, S.-A. Chen, S.-H. Chen and A.-C. Su, *J. Am. Chem. Soc.*, 2005, **127**, 14576.
- 5 J. Liu, J. H. Zou, W. Yang, H. B. Wu, C. Li, B. Zhang, J. B. Peng and Y. Cao, *Chem. Mater.*, 2008, **20**, 4499.
- 6 (a) J. Wang, C.-Q. Zhang, C.-M. Zhong, S.-J. Hu, X.-Y. Chang, Y.-Q. Mo, X. Chen and H.-B. Wu, *Macromolecules*, 2011, **44**, 17; (b) Y.-Q. Mo, X.-Y. Deng, X. Jiang and Q.-H. Cui, *J. Polym. Sci., Part A: Polym. Chem.*, 2009, **47**, 3286.
- 7 L. Wang, Y. Jiang, J. Luo, Y. Zhou, J. Zhou, J. Wang, J. Pei and Y. Cao, *Adv. Mater.*, 2009, **21**, 4854.
- 8 Q.-D. Liu, J. P. Lu, J. F. Ding, M. Day, Y. Tao, P. Barrios, J. Stupak, K. Chan, J. J. Li and Y. Chi, *Adv. Funct. Mater.*, 2007, **17**, 1028.
- 9 (a) C. W. Tang and S. A. Vanslyke, *Appl. Phys. Lett.*, 1987, **51**, 913; (b) S. A. Vanslyke, C. H. Chen and C. W. Tang, *Appl. Phys. Lett.*, 1996, **69**, 2160; (c) S. Tao, L. Li, J. S. Yu, Y. D. Jiang, Y. C. Zhou, C.-S. Lee, S.-T. Lee, X. H. Zhang and O. Kwon, *Chem. Mater.*, 2009, **21**, 1284.
- 10 Y. T. Tao, Q. Wang, L. Ao, C. Zhong, J. G. Qin, C. L. Yang and D. G. Ma, *J. Mater. Chem.*, 2010, **20**, 1759.
- 11 (a) J. P. Lu, Y. N. Jin, J. F. Ding, Y. Tao and M. Day, *J. Mater. Chem.*, 2006, **16**, 593; (b) J. P. Lu, Y. Tao, M. D'iorio, Y. N. Li, J. F. Ding and M. Day, *Macromolecules*, 2004, **37**, 2442.
- 12 (a) C. Ego, A. C. Grimsdale, F. Uckert, G. Yu, G. Srdanov and K. Müllen, *Adv. Mater.*, 2002, **14**, 809; (b) T. Miteva, A. Meisel, W. Knoll, H. G. Nothofer, U. Scherf, D. C. Müller, K. Meerholz, A. Yasuda and D. Neher, *Adv. Mater.*, 2001, **13**, 565; (c) J. P. Chen, D. Markiewicz, V. Y. Lee, G. Klaerner, R. D. Miller and J. C. Scott, *Synth. Met.*, 1999, **107**, 203; (d) W.-L. Yu, J. Pei, W. Huang and A. J. Heeger, *Chem. Commun.*, 2000, 681.
- 13 C. Fan, Y. H. Chen, Z. Q. Jiang, C. L. Yang, C. Zhong, J. G. Qin and D. G. Ma, *J. Mater. Chem.*, 2010, **20**, 3232.
- 14 C.-C. Wu, T.-L. Liu, W.-Y. Hung, Y.-T. Lin, K.-T. Wong, R.-T. Chen, Y.-M. Chen and Y.-Y. Chien, *J. Am. Chem. Soc.*, 2003, **125**, 3710.
- 15 (a) Z. K. Peng, S. Tao, X. H. Zhang, J. X. Tang, C. S. Lee and S.-T. Lee, *J. Phys. Chem. C*, 2008, **112**, 2165; (b) J. Salbeck, N. Yu, J. Bauer, F. Weissortel and H. Bestgen, *Synth. Met.*, 1997, **91**, 209.
- 16 J. A. Mikroyannidis, H. A. Moshopolou, J. A. Anastasopoulos, M. M. Stylianakis, L. Fenenko and C. Adachi, *J. Polym. Sci., Part A: Polym. Chem.*, 2006, **44**, 6790.
- 17 J. F. Ding, M. Day, G. Robertson and J. Roovers, *Macromolecules*, 2002, **35**, 3474.
- 18 (a) D. M. Leeuw, M. M. J. Simenon, A. R. Brown and R. E. F. Einerhand, *Synth. Met.*, 1997, **87**, 53; (b) Y. F. Li, Y. Cao, J. Gao, D. L. Wang, G. Yu and A. J. Heeger, *Synth. Met.*, 1999, **99**, 243; (c) J. Pommerehne, H. Vestweber, W. Guss, R. F. Mahrt, H. Bässler, M. Porsch and J. Daub, *Adv. Mater.*, 1995, **7**, 551.
- 19 K. R. J. Thomas, J. T. Lin, Y.-T. Tao and C.-W. Ko, *J. Am. Chem. Soc.*, 2001, **123**, 9404.
- 20 H. Yan, Q. L. Huang, J. Cui, J. G. C. Veinot, M. M. Kern and T. J. Marks, *Adv. Mater.*, 2003, **15**, 835.
- 21 R. Guan, Y. H. Xu, L. Ying, W. Yang, H. B. Wu, Q. L. Chen and Y. Cao, *J. Mater. Chem.*, 2009, **19**, 531.
- 22 K. R. J. Thomas, J. T. Lin, Y.-T. Tao and C.-H. Chuen, *Chem. Mater.*, 2004, **16**, 5437.
- 23 J. F. Fang, B. H. Wallikewitz, F. Gao, G. L. Tu, C. Muller, G. Pace, R. H. Friend and W. T. S. Huck, *J. Am. Chem. Soc.*, 2011, **133**, 683.
- 24 C.-W. Huang, K.-Y. Peng, C.-Y. Liu, T.-H. Jen, N.-J. Yang and S.-A. Chen, *Adv. Mater.*, 2008, **20**, 3709.
- 25 K. Okumoto, H. Kanno, Y. Hamaa, H. Takahashi and K. Shibata, *Appl. Phys. Lett.*, 2006, **89**, 063504.